Available online at www.sciencedirect.com
ScienceDirect
Ceramics International 37 (2011) 3307–3315
CERAMICS INTERNATIONAL
www.elsevier.com/locate/ceramint

Spontaneously ordered TiO_2 nanostructures

S. Sankar [a], K.G. Gopchandran [a,*], P. Kuppusami [b], S. Murugesan [b]

[a] Department of Optoelectronics, University of Kerala, Trivandrum 695581, India
[b] Physical Metallurgy Division, Indira Gandhi Centre for Atomic Research, Kalpakkam, India

Received 21 December 2010; received in revised form 1 February 2011; accepted 4 April 2011
Available online 31 May 2011

Abstract

Titanium dioxide thin films were deposited on quartz substrates kept at different O_2 pressures using pulsed laser deposition technique. The effects of reactive atmosphere and annealing temperature on the structural, morphological, electrical and optical properties of the films are discussed. Growth of films with morphology consisting of spontaneously ordered nanostructures is reported. The films growth under an oxygen partial pressure of 3×10^{-4} Pa consist in nanoislands with voids in between them whereas the film growth under an oxygen partial pressure of 1×10^{-4} Pa, after having being subjected to annealing at 500 °C, consists in nanosized elongated grains uniformly distributed all over the surface. The growth of nanocrystallites with the increase in annealing temperature is explained on the basis of the critical nuclei-size model.

Keywords: A. Grain growth; C. Optical properties; D. TiO_2; Nanostructures

1. Introduction

Synthesis of semiconductor nanostructures holds considerable technological promise for device applications and energy production. Ordered nanostructures have been extensively studied raising new possibilities at the nanoscale and have been found to exhibit a broad range of enhanced mechanical, optical, magnetic, and electronic properties. Well-ordered nanostructures of TiO_2 is a promising material for photonic and photoelectrochemical applications, because of its high refractive index, chemical stability, and remarkable photocatalytic activity. Nanostructured TiO_2 thin films have many important applications in photocatalysis, photovoltaic devices in solar cells, gas sensors and antireflective coatings [1,2]. These applications are found to strongly depend on the phase, morphology, average particle size and size distribution. TiO_2 is known to crystallize in three different crystallographic structures: rutile (tetragonal), anatase (tetragonal), and brookite (orthorhombic). Brookite and anatase transform to rutile over a wide range of temperatures. The rate and activation energy of anatase–rutile transformation are greatly affected by the concentration of oxygen vacancies or interstitials [3]. Small amounts of oxygen addition in the growing surrounding atmosphere is necessary for depositing nanostructured films having the compositional, structural, and optical characteristics including the stoichiometric composition, good optical transmittance, smooth surface morphology and strong resistance to moisture absorption. Oxygen vacancies and grain boundaries are the main defects of nanostructured TiO_2 films. Oxygen annealing can decrease the oxygen vacancies and passivate the grain boundaries. Annealing temperature is hence a key factor influencing the microstructure and optical properties of nanostructured TiO_2 thin films [4]. The microstructural changes occurring during annealing lead to the decrease in the stored energy due to plastic deformation [5]. In this paper, we report the synthesis of spontaneously ordered nano structures of TiO_2 of amorphous, anatase and rutile phases as thin films on amorphous quartz substrates by employing pulsed laser deposition. Pulsed laser deposition (PLD) is a relatively simple and versatile method for producing metal oxide nanostructures [6]. Effect of reactive O_2 atmosphere during deposition and post deposition annealing on structural, morphological, optical and electrical properties of these structures is discussed in detail.

2. Experimental

TiO_2 thin films were deposited using pulsed laser deposition by employing a Q switched Nd:YAG laser at wavelength of

* Corresponding author. Tel.: +91 471 2308167.
E-mail address: gopchandran@yahoo.com (K.G. Gopchandran).

0272-8842/$36.00
doi:10.1016/j.ceramint.2011.04.126

532 nm with 150 mJ of laser energy, pulse duration of 8 ns and repetition frequency of 10 Hz. The pellets used in this ablation process were prepared from 99.99% pure titanium dioxide powder. Pellets were sintered at a temperature of 1000 °C and pressure of 1×10^5 Pa for 4 h. Before starting the ablation process, the base pressure in the deposition chamber was brought down to $\sim\times 10^{-8}$ Pa. Pure oxygen was circulated in the evacuated chamber through a gas inlet valve and films were deposited in reactive atmosphere of different oxygen pressures in the range 1–5 $\times 10^{-4}$ Pa. Uniform ablation was ensured by rotating the target at constant speed of 90 rpm. Fused amorphous quartz plates of 2 cm × 1 cm × 1 mm size were used as substrates. Substrate–target distance was kept at 4 cm and the time of deposition was 45 min. The obtained films were annealed at different temperatures T_A in the range from 30 to 1000 °C for duration of 1 h. The crystallinity of the films was analyzed using Grazing Incidence X-ray Diffraction (GIXRD) measurements (INEL, France, with Cu K alpha radiation). Raman spectroscopic analyses were conducted using a laser power of 150 mW with Bruker RFS 100/S instrument (Bruker Optics Korea Co. Ltd., S. Korea). The surface morphology of the films was investigated using scanning electron microscopy (SEM) technique using the system Sirion (FEI, USA) in SE mode. Optical measurements were conducted in the wavelength range of 300–900 nm using a double beam UV-Visible spectrophotometer (model V-550, Jasco USA). The electric resistivity of the films at room temperature was measured using four-probe method with current source meter model 6430 (Keithley, USA).

3. Results and discussion

3.1. X-ray diffraction analyses

All as-deposited films showed amorphous nature in GIXRD analysis irrespective of the O_2 partial pressure during the deposition of the films (not shown). This amorphous nature is due to the low mobility of particles impinging on the substrates kept at room temperature, causing very low surface diffusion. Substrate temperature and energy of the particles impinging on the substrate are indeed the relevant parameters in determining the crystalline nature of the as deposited film [7,8].

GIXRD patterns of films deposited at different O_2 pressures, after subjected to annealing at 750 °C, are shown in Fig. 1. For films deposited under lower oxygen partial pressures ($<2 \times 10^{-4}$ Pa), along with dominant anatase phase, formation of rutile phase along R(1 1 0) crystal plane is observed. It has already been reported that TiO_2 films prepared using sputtering technique at lower oxygen pressure (20% O_2 in a total pressure of 0.27 Pa) consists in a mixture of anatase and rutile phases, and at higher oxygen pressure, the film has only the anatase phase and the preferred orientation is along the (1 0 1) crystal plane [9]. At lower partial pressures of O_2, ablated particles can deposit, with fewer collisions with the O_2 molecules of the medium, at the substrate with high kinetic ejection energy equivalent to the formation temperature of the resulting phase. For films deposited under higher oxygen partial pressures ($>2 \times 10^{-4}$ Pa), when subjected to annealing at 750 °C, grain

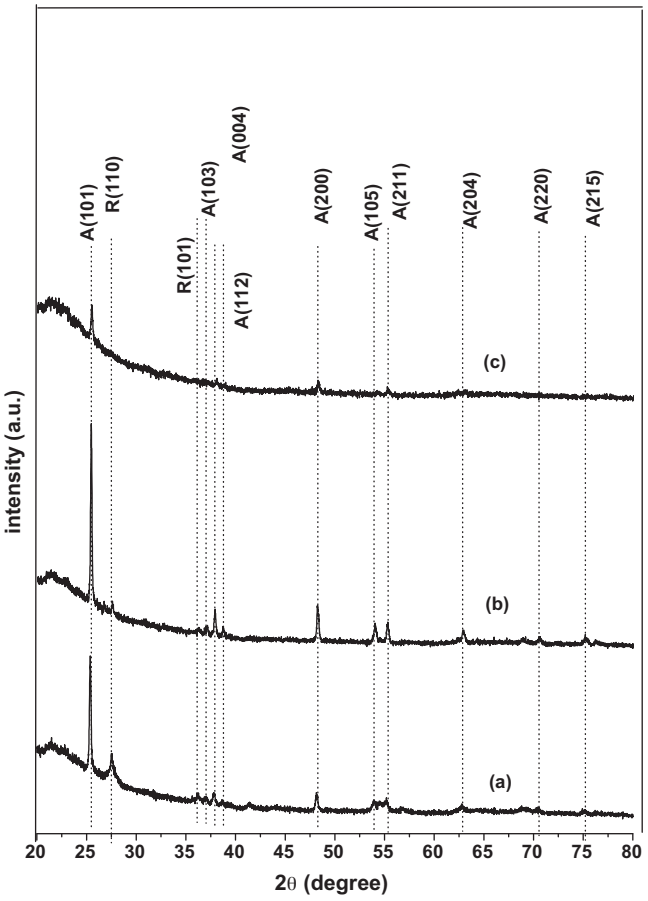

Fig. 1. GIXRD pattern of films deposited at different O_2 pressures of (a) 1×10^{-4} Pa, (b) 3×10^{-4} Pa, and (c) 5×10^{-4} Pa; after annealing at 750 °C.

growth with anatase phase with preferential growth along A (1 0 1) crystal plane is observed.

GIXRD patterns of films deposited at different O_2 pressures, after having being subjected to annealing at 1000 °C, are shown in Fig. 2. Intensities of X-ray diffraction peaks are found to increase for films deposited at higher O_2 partial pressures, when annealed at 1000 °C. The relative intensity of the R (1 0 1) peak is found to increase with the increase in O_2 pressure while that of the R (1 1 0) diminishes, as shown in Fig. 2, indicating a favourable condition for growth on the (1 0 1) plane. The energy of the particles impinging on the substrate is an important parameter affecting the film microstructure [10]. Even after annealing, the preferred orientation is often determined by thermodynamic constraints during deposition. Anatase crystallites were also observed in the film deposited at 3×10^{-4} Pa O_2 even after annealing at 1000 °C. The brookite phase has not been observed in any of the films investigated.

The crystallite size of the preferentially oriented crystal planes are calculated using the Debye Scherrer formula [11]:

$$D = \frac{K\lambda}{\beta\cos\theta} \quad (1)$$

where K is the shape factor, θ the Bragg's diffraction angle in radian, β the broadening of diffraction line at half its maximum

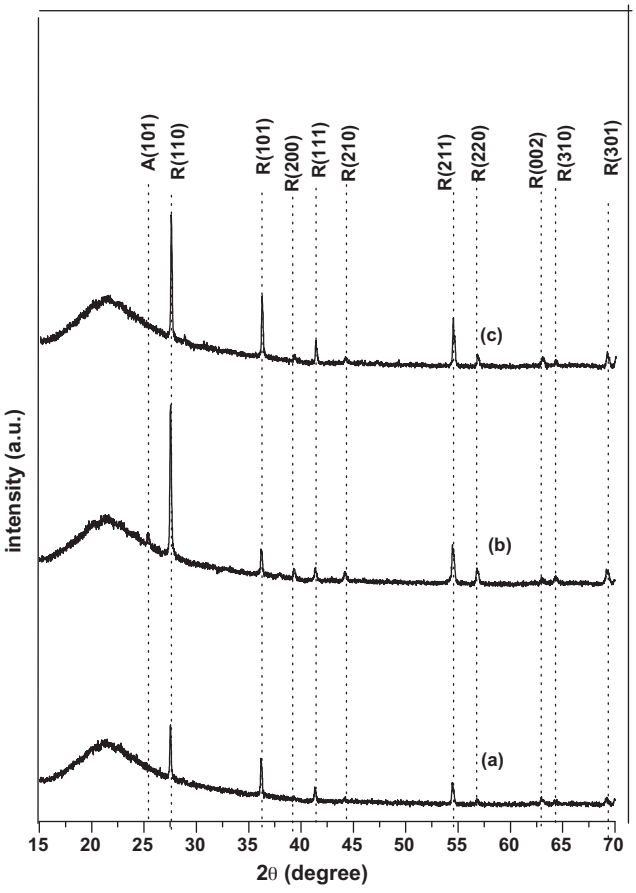

Fig. 2. GIXRD pattern of films deposited at different O_2 pressures of (a) 1×10^{-4} Pa, (b) 3×10^{-4} Pa, and (c) 5×10^{-4} Pa; after annealing at 1000 °C.

intensity (FWHM) in radian and λ the wavelength of X-rays used. Crystallite size associated with different thin film samples are given in Table 1.

The GIXRD patterns of the films annealed at different temperatures are shown in Fig. 3. Annealing at 500 °C resulted in the formation of pure anatase phase with preferential orientation along (1 0 1) plane. Films annealed at 750 °C exhibited a mixed phase with growth along (1 0 1) and (2 0 0) planes of anatase and (1 1 0) and (0 0 2) planes of rutile. Film annealed at 1000 °C exhibited rutile phase with preferential growth along (1 1 0) plane. Anatase-to-rutile transformation involves an overall contraction or shrinking of the oxygen structure and a co-operative movement of oxygen and titanium ions. At high temperatures, it is possible for the phase transition to overcome strain energy for the oxygen ions to reach their new configuration by breaking the Ti–O bonds [12]. Rutile has minimum free energy in comparison with other titania polymorphs. Hence, by annealing at elevated temperatures, required activation energy is provided so that all other polymorphs including anatase transform into rutile through first-order phase transformation. However, the temperature at which metastable anatase to stable rutile transformation takes place depends upon several factors, including impurities present in the anatase, primary particle size, texture and strain in the structure. Hence, porosity and/or surface area reduction can occur due to the sintering effects associated with nucleation-growth type of phase transformations [13–15]. The variation of crystallite average size with annealing temperature is given in Table 1. Crystallite average size is found to increase with the increase in annealing temperature:

Table 1
Different structural parameters as a function of annealing temperature and O_2 partial pressure.

O_2 pressure (10^{-4} Pa)	Annealing temperature (°C)	Phase identified (A—anatase, R—rutile)	Interplanar spacing d (Å)	Grain size D (nm)	Lattice constants (Å)
1		A (1 0 1)	3.5060	33.74	Anatase:
	500	A (2 0 0)	1.8897	29.31	$a = 3.7794$
					$c = 9.3889$
		A (1 0 1)	3.5060	44.54	Anatase:
	750	A (1 0 3)	2.3783	23.44	$a = 3.7766$
		A (2 0 0)	1.8883	41.55	$c = 9.4320$
		R (1 1 0)	3.2397	17.43	Rutile:
					$a = 4.5816$
					$c = 2.9980$
		R (1 1 0)	3.2388	56.28	Rutile:
	1000	R (1 0 1)	2.4820	44.02	$a = 4.5803$
		R (1 1 1)	2.1843	28.61	$c = 2.9532$
3		A (1 0 1)	3.5054	61.28	Anatase:
	750	A (2 0 0)	1.8856	32.96	$a = 3.7712$
					$c = 9.5056$
		R (1 1 0)	3.2331	56.32	Rutile:
	1000	R (1 0 1)	2.4737	62.32	$a = 4.5723$
		R (2 1 1)	1.6845	31.99	$c = 2.9423$
		A (1 0 1)	3.4940	36.45	Anatase:
5	750	A (2 0 0)	1.8856		$a = 3.7712$
					$c = 9.2851$
	1000	R (1 1 0)	3.2263	56.28	Rutile:
		R (1 0 1)	2.4706	44.00	$a = 4.5627$
		R (2 1 1)	1.6808	36.35	$c = 2.9387$

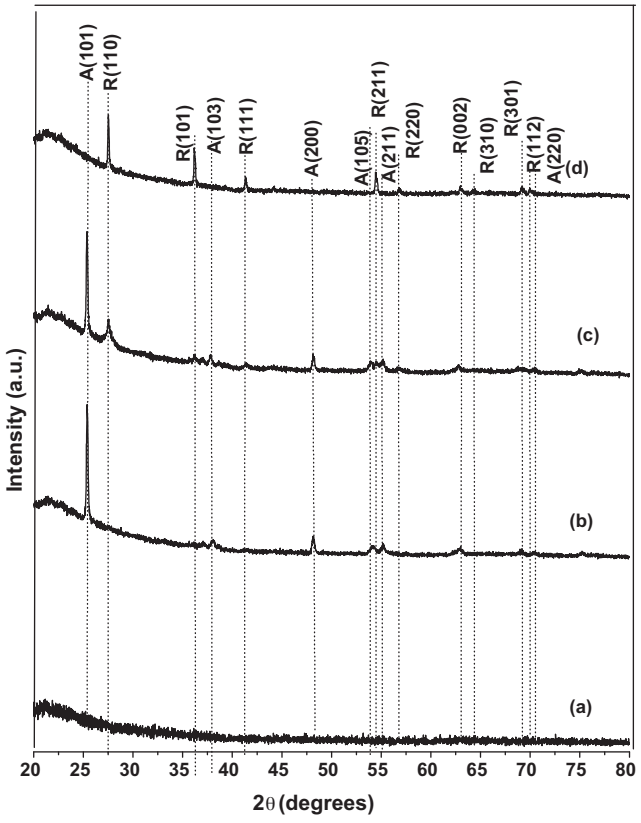

Fig. 3. GIXRD pattern of films deposited at O_2 pressure of 1×10^{-4} Pa and subjected to annealing at (a) 30 °C, (b) 500 °C, (c) 750 °C and (d) 1000 °C.

the smaller crystallites tend to have surfaces with sharper convexity and gradually by coalescence very likely the larger crystallites [16]. Although both anatase and rutile phases have tetragonal crystalline structure, there is a difference in the lattice parameter making the anatase phase less dense than the rutile phase. This fact explains the difference in the refractive index values for these phases [17]. The lattice constant a and c were found to agree well with bulk values [18]. The films annealed at 750 °C showed mixed phase of anatase and rutile. In mixed phase films, weight percentage of anatase phase, W_A was calculated using the relation deduced by Spurr and Mayers [19], as follows:

$$W_A = \frac{1}{(1 + 1.265((I_R)/(I_A)))} \quad (2)$$

where I_A and I_R are intensities of A (1 0 1) anatase peak and R (1 1 0) rutile peak, respectively. Under such approximation, the weight percentage of the anatase phase was found to be 64%.

3.2. Raman spectroscopic analyses

Raman spectra of films deposited at different O_2 partial pressures, after subjected to annealing at 750 and 1000 °C, are shown in Figs. 4 and 5, respectively. Raman spectra of films, deposited on substrates kept at room temperature under oxygen partial pressure of 1×10^{-4} Pa, after subjected to annealing at different temperatures is shown in Fig. 6.

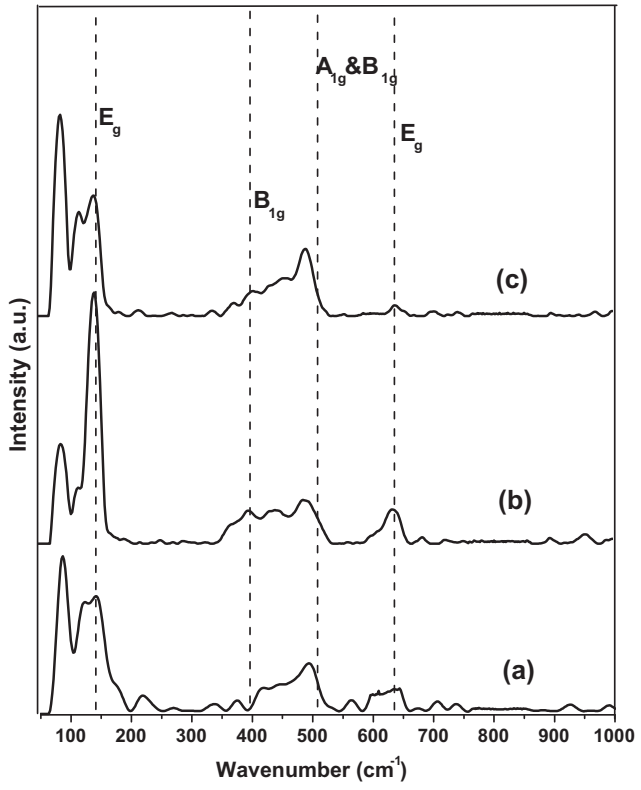

Fig. 4. Raman spectra of films, after subjected to annealing at 750 °C deposited on substrates kept at room temperature and at O_2 partial pressures of 1×10^{-4} Pa, (b) 3×10^{-4} Pa, and (c) 5×10^{-4} Pa.

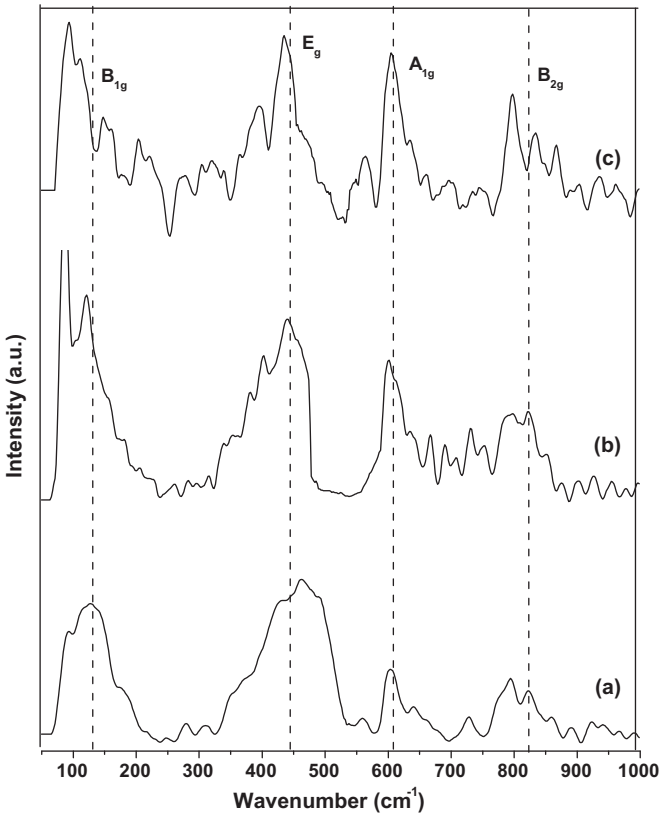

Fig. 5. Raman spectra of films, after subjected to annealing at 1000 °C deposited on substrates kept at room temperature and at O_2 partial pressures of 1×10^{-4} Pa, (b) 3×10^{-4} Pa, and (c) 5×10^{-4} Pa.

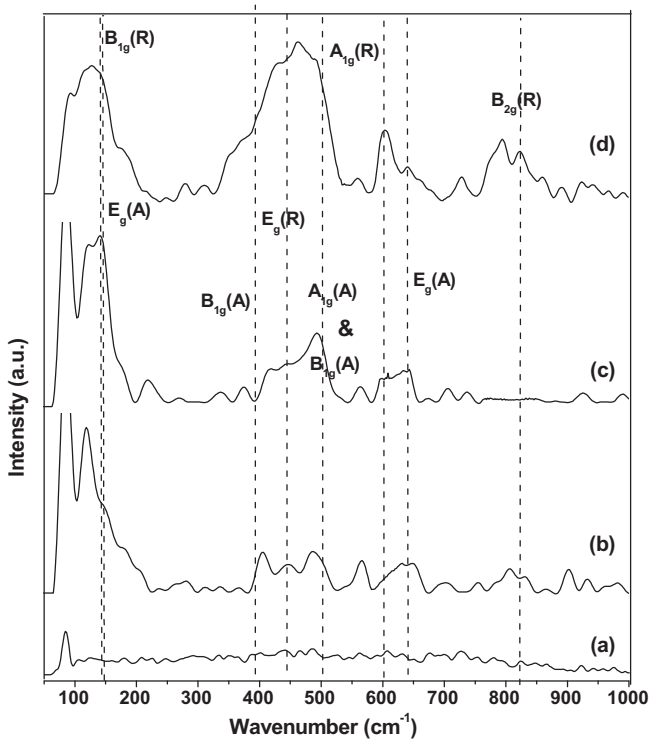

Fig. 6. Raman spectra of films deposited at O_2 pressure of 1×10^{-4} Pa after subjected to annealing at (a) 30 °C, (b) 500 °C, (c) 750 °C and (d) 1000 °C.

The Raman spectra indicate that all films annealed at 750 °C are made of anatase TiO_2 phase. The Raman lines at 145, 399, 516 and 640 cm^{-1} are corresponding to the E_g, B_{1g}, A_{1g} or B_{1g}, and E_g vibrational modes of bulk anatase TiO_2. All the Raman lines are found to be slightly redshifted from the bulk values except for the E_g mode at 640 cm^{-1}. The slight shift observed in the Raman lines can be attributed to the refinement in crystallite size to the nanometer range together with a high density of defects in thin films [20]. The most intense Raman line is observed corresponding to E_g mode at 145 cm^{-1} for all these films. This low frequency mode of anatase corresponds to O–Ti–O bending vibration in the TiO_6 octahedra [21]. The separation distance between the two oxygen atoms involved in this bending is very large (3.04 Å). It will result in weak repulsion interaction between these two oxygen atoms and contribute maximum intensity to Raman line corresponding to E_g mode at 145 cm^{-1}. The strongest Raman lines are observed for the film deposited at 3×10^{-4} Pa of O_2 and annealed at 750 °C. The Raman spectra of all the films annealed at 1000 °C are found to be of rutile TiO_2 phase. The frequencies corresponding to Raman active modes in bulk rutile TiO_2 are 143 cm^{-1} (B_{1g}), 447 cm^{-1} (E_g), 612 cm^{-1} (A_{1g}) and 826 cm^{-1} (B_{2g}) [22]. Raman peaks are observed to be sharpened and redshifted for the films deposited under increased oxygen partial pressures after subjected to annealing at 1000 °C. Maximum intensity is observed for the E_g mode at 447 cm^{-1} for all these films. Bandwidth and frequency shift of Raman lines can be attributed to extend of non-stoichiometry by oxygen deficiencies or the disorder induced by minor phases, pressure and phonon confinement effects. It is well established that non-stoichiometry strongly affect the lattice vibrational characteristics and induces the line shape change of Raman lines in oxides. Frequency shift and broadening of Raman lines can also be attributed to the decrease in the crystalline dimension to the nanometer regime and phonon confinement [23,24].

The structural evolution of crystalline phases of TiO_2 thin films as a function of annealing temperature and the anatase to rutile transformation is clearly evident from the Raman spectra shown in Fig. 6.

3.3. SEM structural analyses

SEM micrographs of the films grown under different conditions are shown in Fig. 7. The morphology of the film is found to change significantly with increase in oxygen partial pressure. Films deposited under low oxygen pressure exhibit a dense microstructure without porosity (Fig. 7(a)). With increase in oxygen pressure, morphology of the film changes to a spontaneously ordered nature with nanoislands with voids of nanoscale dimensions in between them (Fig. 7(b)). The significant modifications of morphology of TiO_2 thin films with increase in background oxygen pressure suggest that oxidation kinetics play a key role in determining the morphology of the films. The laser ablation of the target in the PLD process ejects highly energetic species, which favours the formation of dense films when the deposition is performed under a high vacuum environment of the order of 10^{-8} Pa. Beside, under higher background pressures of the order of 10^{-4} Pa, the ablated species undergo several collisions with the oxygen atoms resulting in enhanced oxidations and in addition reach at the substrate with a much lower energy, which limits their surface mobility and consequently leads to structures as shown in Fig. 7(b) [25].

The influence of the annealing temperature on the surface morphology has also been studied. It can be seen from the SEM micrographs that the morphology of the thin films changes drastically with increase in annealing temperature. Fig. 7(c) and (d) shows the surface morphology of TiO_2 films deposited in O_2 partial pressure of 1×10^{-4} Pa after subjected to annealing at 500 and 750 °C, respectively. Surface morphology of the film annealed at 500 °C is found to be of nanosized elongated grains in an ordered fashion. These crystallites are confirmed as that of anatase phase in GIXRD analysis. Grain size is found to increase significantly with annealing above this temperature. Film annealed at 750 °C is found to be consisting of agglomerated nanocrystals. These crystallites are confirmed as that of mixed phase with anatase domination. It can be seen that when the annealing temperature reaches 1000 °C (Fig. 7(e)), there is a distinct change of surface morphology. Fig. 7(e) shows that previously observed column-like nodules, now have facets. In addition, the size of the particles is found to increase drastically. From GIXRD analysis it can be concluded that TiO_2 film annealed at 1000 °C has changed into rutile structure completely (Fig. 2(a)).

During annealing, the anatase nanocrystals coarsen and when their size reaches a critical value they transform to stable

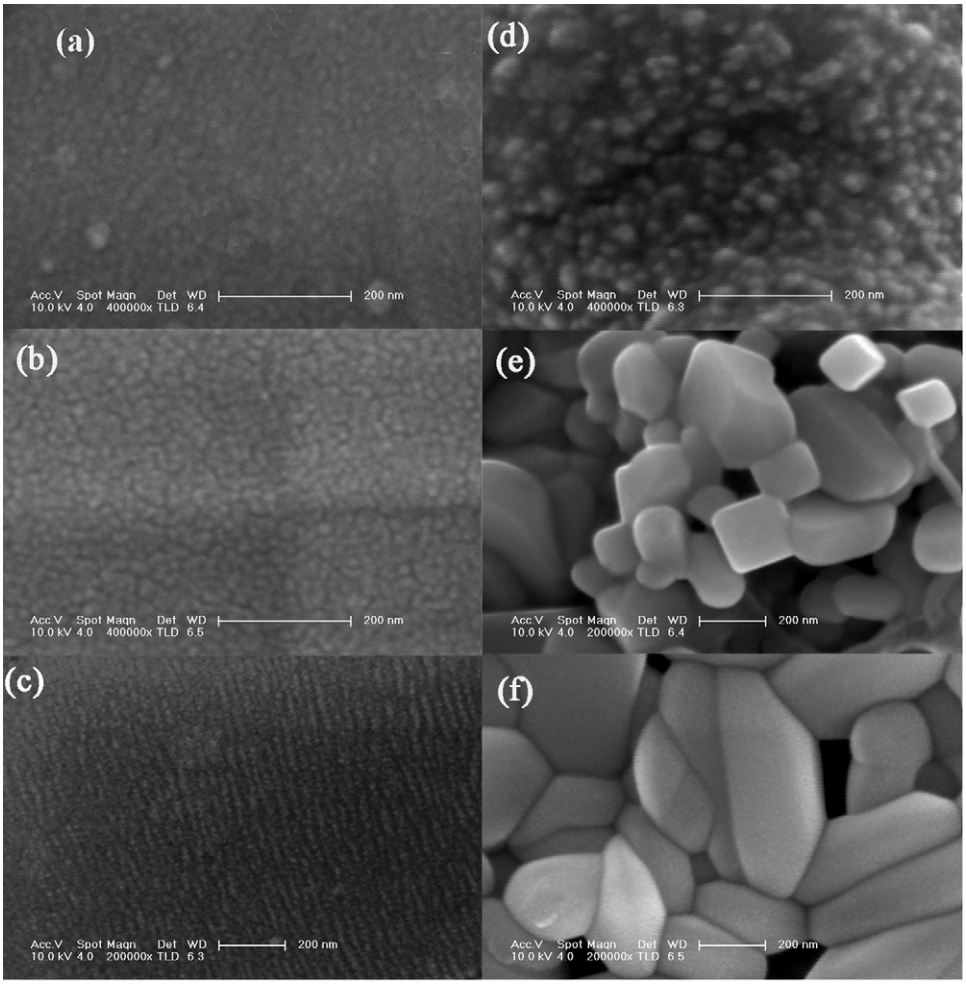

Fig. 7. SEM micrographs of films deposited at different O_2 pressures and annealing temperatures: (a) 1×10^{-4} Pa and 30 °C, (b) 3×10^{-4} Pa and 30 °C, (c) 1×10^{-4} Pa and 500 °C, (d) 1×10^{-4} Pa and 750 °C, (e) 1×10^{-4} Pa and 1000 °C, (f) 3×10^{-4} Pa and 1000 °C.

rutile phase. This behaviour has been described by the critical nuclei-size model [26]. According to this model the rutile crystallites cannot grow until the nucleus size of this phase reaches a critical value; this requires an agglomeration of fine-grained anatase particles into larger ones. The growth of anatase nanocrystallites beyond the critical size is energetically not favourable since anatase has a higher total energy compared to rutile. Further growth of anatase grains during thermal annealing above 750 °C is unlikely and the transformation to rutile takes place. In contrast to the anatase, the rutile grains grow very fast during the annealing above this temperature. Only grains with a certain orientation are preferentially reacting with oxygen. Several studies on (1 1 0) rutile surface reactivity have shown that in the presence of oxygen, the surface reconstruction is achieved by the growth of various types of structures [27–29]. The changes in the (1 1 0) surface led to a structure of terraces that is formed after annealing in oxygen at 1000 °C [30]. Fig. 7(f) shows the surface morphology of the film deposited in O_2 partial pressures of 3×10^{-4} Pa after subjected to annealing at 1000 °C. It consists in elongated large closely packed grains.

3.4. UV–vis spectroscopic studies

Optical transmittance spectra of as deposited films at different O_2 pressures are shown in Fig. 8. Optical transmittance is found to increase with the increase in O_2 pressure of the reactive atmosphere. For the as deposited films with maximum transmittance, refractive indices at different wavelengths were calculated. Dispersion of refractive index of these films was fitted using the single oscillator-Wemple and Didomenico model [31–33]. The oscillator energy E_0 and the strength of inter band optical transition of dispersion energy E_d were found out for films deposited at 0.05 mbar as 5.8 and 28.97 eV, respectively.

In the vicinity of the fundamental absorption, the absorption edge was calculated as follows:

$$(\alpha h\nu) = A(h\nu - E_g)^m \quad (3)$$

where A is the edge width parameter representing the film quality, calculated from the linear part of the relation, E_g is the optical energy gap of the material and m determines the type of transition. The absorption coefficient can be calculated from

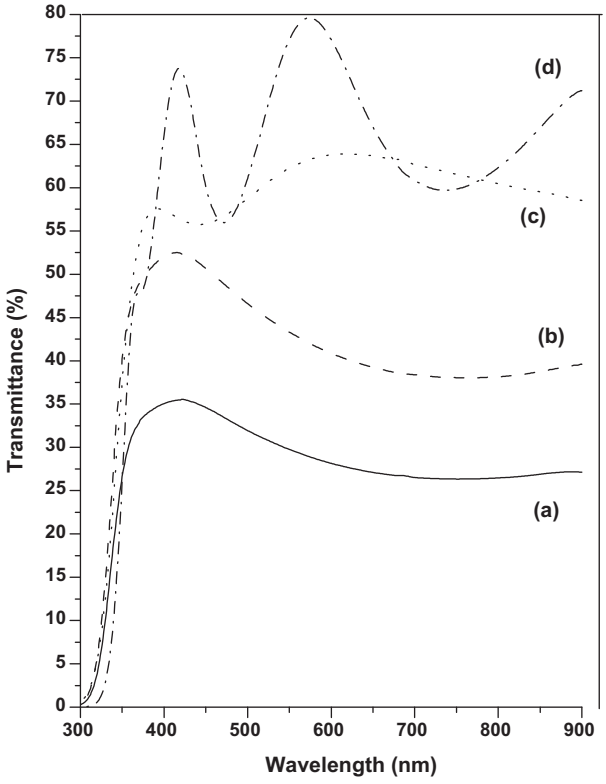

Fig. 8. Transmittance spectra of films deposited at different O_2 pressures of (a) 1×10^{-4} Pa, (b) 2×10^{-4} Pa, (c) 3×10^{-4} Pa and (d) 5×10^{-4} Pa.

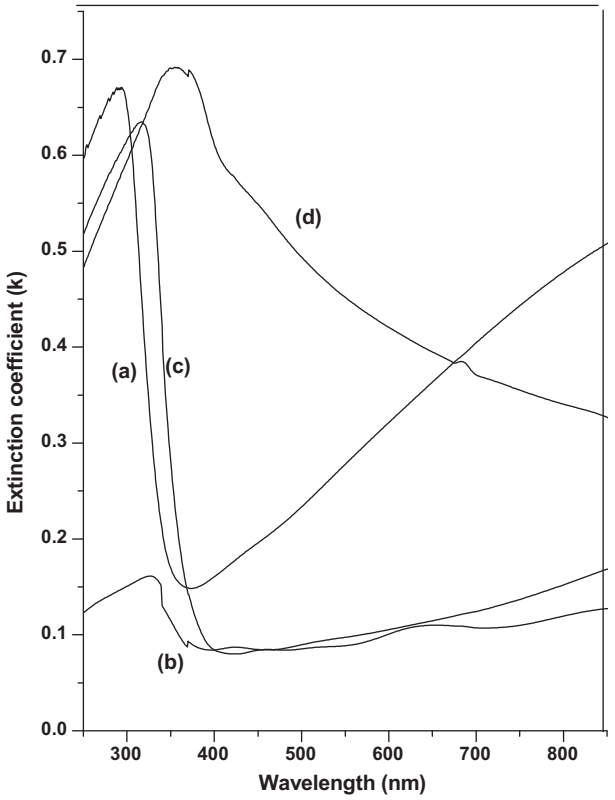

Fig. 9. A plot of extinction coefficient against λ for films deposited at O_2 pressure of 1×10^{-4} Pa after subjected to annealing at (a) 30 °C, (b) 500 °C, (c) 750 °C and (d) 1000 °C.

Lambert's formula as follows:

$$\alpha = \left(\frac{1}{t}\right)\ln\left(\frac{1}{T}\right) \tag{4}$$

where T is the transmittance and t is the thickness of the film. The value of m is 1/2 for direct allowed, 2 for indirect allowed, 3/2 for direct forbidden and 3 for indirect forbidden transition [34]. The correct value for m is found as corresponding to the best fit.

The optical band gap values E_g of the as deposited films were obtained from a plot of $(\alpha h\nu)^{1/2}$ vs. $h\nu$ and is given in Table 2.

Table 2
Variation in optical band gap of thin films as a function of annealing temperature and O_2 partial pressure.

Annealing temperature (°C)	O_2 pressure (10^{-4} Pa)	Band gap (eV)
30	1	3.21
	2	3.26
	3	3.16
	5	3.23
750	1	3.11
	2	3.18
	3	3.25
	5	3.27
1000	1	2.92
	2	2.98
	3	3.06
	5	3.14

The extinction coefficient was also calculated for different wavelengths λ as follows:

$$k = \frac{\alpha\lambda}{4\pi} \tag{5}$$

A plot of extinction coefficient against λ is shown in Fig. 9.

It can be seen that even after annealing at high temperatures, reactive atmosphere during deposition has a vital role in determining the transmittance of the films. Optical transmittance is found to be increased with annealing temperature in the 300–750 °C range. Maximum transmittance is observed for the film annealed at 750 °C. But the films annealed at 1000 °C exhibited the minimum transmittance. The sharp decrease in the transparency of TiO_2 thin films in the UV region is caused by the fundamental light absorption. The optical properties of these films can be explained by the phase transformation and the growth of crystallites taking place during deposition and annealing. X-ray diffraction investigations showed that as-deposited TiO_2 films obtained are amorphous, which often contains many structural defects. On annealing at lower temperatures, the TiO_2 films become denser and change into anatase structure. The structural defects in TiO_2 films decreased and the crystal grains did not get very coarse. So, the TiO_2 film annealed at 750 °C has the best optical property. After that, the crystallites grow and will become coarser. The sudden decrease in transmission observed at 1000 °C can be attributed to the phase transformation.

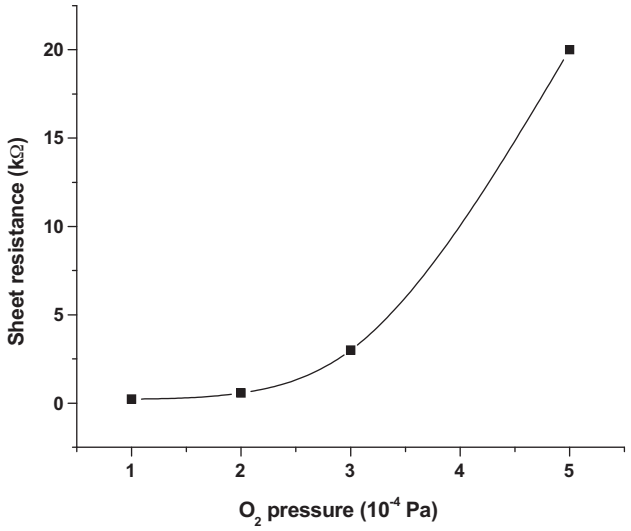

Fig. 10. Variation of sheet resistance of the as deposited films with oxygen pressure.

Optical band gap of the films annealed at different temperatures were found out using Eq. (3). Variation of $(\alpha h\nu)^{1/2}$ vs. $h\nu$ graph for the films were plotted. The values of energy gap E_g for indirect allowed transitions are determined from the intercepts of the extrapolation to zero absorption to photon energy axis (Table 2).

3.5. Electric characterization

Variation of sheet resistance of the as-deposited films with oxygen pressure is shown in Fig. 10. Sheet resistance was found to increase with the increase in O_2 pressure. General formula of titanium oxides can be represented by the formula Ti_mO_{2m-1} ($m = 1$ to ∞) and they exhibit a variety of electrical properties depending on the oxidation state. For example, TiO shows superconductivity [35] and stoichiometric TiO_2 acts as an insulator. It is well known that the electrical conductivity of TiO_2 is markedly affected by the oxygen defects. Semiconductivity is caused by introduction of oxygen defects into the TiO_2 structure [36]. After annealing processes as discussed in preceding sections at 750 and 1000 °C, all the films were found to be changed to dielectric.

4. Conclusions

The structural, morphological, optical and electrical properties of titanium oxide thin films are found to be strongly influenced by the thermodynamics involving reactive atmosphere during deposition and annealing temperature. Growth of films with morphology consisting of spontaneously ordered nanostructures is reported. The films grown under an oxygen partial pressure of 3×10^{-4} Pa consist in nanoislands with voids between them and the films grown under an oxygen partial pressure of 1×10^{-4} Pa, after subjected to annealing at 500 °C, consists in nanosized elongated grains uniformly distributed all over the surface. Annealing at higher temperatures resulted in morphology with larger grains. The growth of nanocrystallites with increase in annealing temperature is explained on the basis of the critical nuclei-size model. In films, subjected to annealing at 750 °C, deposited at room temperature under lower oxygen partial pressures ($<2 \times 10^{-4}$ Pa), along with dominant anatase phase, formation of rutile phase with preferred orientation for (1 1 0) plane was also observed. Phase transformation from amorphous to anatase, anatase to mixed and then to rutile TiO_2 with annealing temperature is described with GIXRD and Raman spectroscopy. Variations in optical properties of TiO_2 thin films prepared with different growth parameters are also studied and the results are correlated with structural and morphological properties of the films. Sheet resistance of the as deposited films was found to increase with increase in O_2 partial pressure and the films became dielectric when subjected to annealing at elevated temperatures.

References

[1] G.K. Mor, O.K. Varghese, M. Paulose, K. Shankar, C.A. Grimes, A review on highly ordered, vertically oriented TiO_2 nanotube arrays: fabrication, material properties, and solar energy applications, Sol. Energy Mater. Solar Cells 90 (2006) 2011–2075.
[2] S.H. Jeong, J.K. Kim, B.S. Kim, S.H. Shim, B.T. Lee, Characterization of SiO_2 and TiO_2 films prepared using rf magnetron sputtering and their application to anti-reflection coating, Vacuum 76 (2004) 507–515.
[3] R.D. Shannon, J.A. Pask, Kinetics of the anatase–rutile transformation, J. Am. Ceram. Soc. 48 (1965) 391–398.
[4] S. Sankar, K.G. Gopchandran, Effect of annealing on the structural, electrical and optical properties of nanostructured TiO_2 thin films, Cryst. Res. Technol. 44 (2009) 989–994.
[5] P.R. Rios, F. Siciliano Jr., H.R.Z. Sandim, R.L. Plaut, A.F. Padilha, Nucleation and growth during recrystallization, Mater. Res. 8 (3) (2005) 225–238.
[6] P. Kuppusami, V.S. Raghunathan, Status of pulsed laser deposition: challenges and opportunities, Surf. Eng. 22 (2) (2006) 81–83.
[7] P. Lobl, M. Huppertz, D. Mergel, Nucleation and growth in TiO_2 films prepared by sputtering and evaporation, Thin Solid Films 251 (1994) 72–79.
[8] S. Murugesan, P. Kuppusami, N. Parvathavarthini, E. Mohandas, Pulsed laser deposition of anatase and rutile TiO_2 thin films, Surf. Coat. Technol. 201 (2007) 7713–7719.
[9] D. Wicaksana, A. Kobayashi, A. Kinbara, Process effects on structural properties of TiO_2 thin films by reactive sputtering, J. Vac. Sci. Technol. A 10 (1992) 1479–1482.
[10] Y.X. Leng, N. Huang, P. Yang, J.Y. Chen, H. Sun, J. Wang, G.J. Wan, Y. Leng, P.K. Chu, Influence of oxygen pressure on the properties and biocompatibility of titanium oxide fabricated by metal plasma ion implantation and deposition, Thin Solid Films 420–421 (2002) 408–413.
[11] B.D. Cullity, Elements of X-ray Diffraction, 2nd ed., Addison Wesley, Reading, MA, 1978.
[12] L. Pauling, The principles of determining the structure of complex ionic crystals, J. Am. Chem. Soc. 51 (1929) 1010–1026.
[13] O.J. Whittemore, J.J. Sipe, Pore growth during the initial stages of sintering ceramics, Powder Technol. 9 (1974) 159–164.
[14] K.N.P. Kumar, K. Keizer, A.J. Burggraaf, Textural evolution and phase transformation in titania membranes: Part 1—Unsupported membranes, J. Mater. Chem. 3 (1993) 1141–1149.
[15] K.N.P. Kumar, K. Keizer, A.J. Burggraaf, T. Okubo, H. Nagamoto, Textural evolution and phase transformation in titania membranes: Part 2—Supported membranes, J. Mater. Chem. 3 (1993) 1151–1159.
[16] H.P. Deshmukh, P.S. Shinde, P.S. Patilb, Structural, optical and electrical characterization of spray-deposited TiO_2 thin films, Mater. Sci. Eng. B 130 (2006) 220–227.

[17] L. Castaneda, J.C. Alonso, A. Ortiz, E. Andrade, J.M. Saniger, J.G. Bañuelos, Spray pyrolysis deposition and characterization of titanium oxide thin films, Mater. Chem. Phys. 77 (2002) 938–944.
[18] Natl. Bur. Stand. (US) Monogr. 25, 1969.
[19] R.A. Spurr, H. Myers, Quantitative analysis of anatase–rutile mixtures with an X-ray diffractometer, Anal. Chem. 29 (1957) 760–762.
[20] Y. Zhang, J. Li, J. Wang, Substrate-assisted crystallization and photocatalytic properties of mesoporous TiO_2 thin films, Chem. Mater. 18 (2006) 2917–2923.
[21] H. Tang, K. Prasad, R. Sanjinbs, P.E. Schmid, F. Levy, Electrical and optical properties of TiO_2 anatase thin films, J. Appl. Phys. 75 (1994) 2042–2047.
[22] P.S. Preecy, B. Morosin, Pressure and temperature dependences of the Raman active phonons in SnO_2, Phys. Rev. B 7 (1973) 2779–2786.
[23] J.C. Parker, R.W. Siegel, Calibration of the Raman spectrum to the oxygen stoichiometry of nanophase TiO_2, Appl. Phys. Lett. 57 (1990) 943–945.
[24] R.J. Nemanich, S.A. Solin, R.M. Martin, Light scattering study of boron nitride microcrystals, Phys. Rev. B 23 (1981) 6348–6356.
[25] M.P. Li-Jian Meng, Dos Santos, The influence of oxygen partial pressure on the properties of DC reactive magnetron sputtered titanium oxide films, Appl. Surf. Sci. 68 (1993) 319–325.
[26] K.N.P. Kumar, Growth of rutile crystallites during the initial stage of anatase-to-rutile transformation in pure titania and in titania-alumina nanocomposites, Scripta Metall. Mater. 32 (1995) 873–877.
[27] S. Gan, Y. Liang, D.R. Baer, Atomic control of TiO_2 (1 1 0) surface by oxygen plasma treatment, Surf. Sci. 459 (2000) L498–L502.
[28] M. Li, W. Hebenstreit, U. Diebold, Oxygen-induced restructuring of the rutile TiO_2 (1 1 0) (1 × 1) surface, Surf. Sci. 414 (1998) L951–L956.
[29] W.S. Epling, C.H.F. Peden, M.A. Henderson, U. Diebold, Evidence for oxygen adatoms on TiO_2 (1 1 0) resulting from O_2 dissociation at vacancy sites, Surf. Sci. 412/413 (1998) 333–343.
[30] M. Li, W. Hebenstreit, L. Gross, U. Diebold, M.A. Henderson, D.R. Jennison, P.A. Schultz, M.P. Sears, Oxygen induced restructuring of the TiO_2 (1 1 0) surface: a comprehensive study, Surf. Sci. 437 (1999) 173–190.
[31] R. Swanepoel, Determination of the thickness and optical constants of amorphous silicon, J. Phys. E: Sci. Instrum. 16 (1983) 1214–1222.
[32] S.H. Wemple, M. DiDomenico Jr., Behavior of the electronic dielectric constant in covalent and ionic materials, Phys. Rev. B 3 (1971) 1338–1351.
[33] M.M. Abdel-Aziz, I.S. Yahia, L.A. Wahab, M. Fadel, M.A. Afifi, Determination and analysis of dispersive optical constant of TiO_2 and Ti_2O_3 thin films, Appl. Surf. Sci. 252 (2006) 8163–8170.
[34] H. Tang, H. Berger, P.E. Schmid, F. Levy, Optical properties of anatase (TiO_2), Solid. State. Commun. 92 (1994) 267–271.
[35] T.B. Reed, M.D. Banus, M. Sjostrand, P.H. Keeson, Superconductivity in cubic and monoclinic "TiO.", J. Appl. Phys. 43 (1972) 2478–2479.
[36] F. Imai, K. Kunimori, T. Manabe, T. Kumagai, H. Nozoye, Epitaxial growth of titanium oxide thin films on MgO(1 0 0) single-crystal substrates by reactive deposition methods, Thin Solid Films 310 (1997) 184–193.